

Spin Symmetry Predictions for Heavy Quarkonia Alignment

Peter Cho¹ and Mark B. Wise²

Lauritsen Laboratory
California Institute of Technology
Pasadena, CA 91125

Abstract

We investigate the implications of spin symmetry for heavy quarkonia production and decay. We first compare spin symmetry predictions for charmonia and bottomonia radiative transitions with data and find they agree quite well. We next use spin symmetry along with nonrelativistic QCD power counting to determine the leading order alignment of P and D-wave orthoquarkonia that are produced through gluon fragmentation. Finally, we discuss a mechanism which may resolve the current factor of 30 discrepancy between theoretical predictions and experimental measurements of prompt ψ' production at the Tevatron. This mechanism involves gluon fragmentation to a subleading Fock component in the ψ' wavefunction and yields 100% transversely aligned ψ' 's to lowest order. Observation of such a large alignment would provide strong support for this resolution to the ψ' problem.

11/94

¹ Work supported in part by a DuBridge Fellowship and by the U.S. Dept. of Energy under DOE Grant no. DE-FG03-92-ER40701.

² Work supported in part by the U.S. Dept. of Energy under DOE Grant no. DE-FG03-92-ER40701.

1. Introduction

Spin symmetry has played an important role in the study of heavy hadrons during the past several years. Many of its consequences for mesons and baryons with quark content $Q\bar{q}$ and Qqq have been investigated within the context of the Heavy Quark Effective Theory (HQET) [1]. The spin and flavor symmetries of QCD that become exact in the $M_Q \rightarrow \infty$ limit are transparent in this effective theory framework. But even without the HQET apparatus, several aspects of charm and bottom hadron phenomenology may be understood from symmetry considerations alone. For example, the rates for strong and electromagnetic transitions between states belonging to separate spin doublets are simply related by group theory factors. Moreover, the sums of partial widths for each member of a doublet to decay to states in another doublet are equal. These predictions that follow from spin symmetry in the infinite mass limit appear to be reasonably well satisfied for finite mass hadrons in the charm and bottom sectors [2].

In this letter, we consider the implications of spin symmetry for heavy quarkonia. Since the spins of both the quark and antiquark inside a $Q\bar{Q}$ bound state are separately conserved as $M_Q \rightarrow \infty$, transitions between members of different quarkonia multiplets within the same flavor sector are more tightly constrained than their heavy-light meson analogues. Ratios of decay rates can be predicted and checked against the large body of charmonia and bottomonia data collected over the past two decades. Spin symmetry also constrains $Q\bar{Q}$ bound state formation and ties in closely with recent perturbative QCD calculations of parton fragmentation to heavy quarkonia [3–6]. As we shall see, the union of these ideas yields several interesting predictions which can be experimentally tested at hadron colliders.

Our paper is organized as follows. We first review the general relation that spin symmetry imposes upon heavy hadron transitions in section 2. We then test this relation for quarkonia by comparing its predictions for $Q\bar{Q}$ electromagnetic transitions with experimental data. In section 3, we use the spin symmetry relation along with nonrelativistic QCD power counting arguments to determine the leading order alignment of P and D-wave orthoquarkonia produced via gluon fragmentation. Finally, we discuss the implications of spin symmetry for a fragmentation mechanism which may resolve the current large discrepancy between theory and experiment in prompt ψ' production at the Tevatron.

2. Radiative Quarkonia Transitions

It is useful to recall the basic symmetry relation which constrains transitions between any initial and final hadronic states H and H' that contain heavy constituents [2]. For $Q\bar{q}$ mesons and Qqq baryons, we let $j_h^{(\prime)}$, $j_\ell^{(\prime)}$ and $J^{(\prime)}$ denote the angular momentum of $H^{(\prime)}$'s heavy, light and total degrees of freedom. As the mass of the heavy constituents inside $H^{(\prime)}$ tends to infinity, the separate angular momenta of the light and heavy degrees of freedom become good quantum numbers. A similar phenomenon occurs for $Q\bar{Q}$ quarkonia. But in this case, the quantum number $j_h^{(\prime)}$ represents just the total spin of the $Q\bar{Q}$ pair, while $j_\ell^{(\prime)}$ stands for the bound state's remaining angular momentum which includes the orbital contribution from the heavy quark and antiquark.

In the infinite mass limit, the amplitude for a general $H \rightarrow H'$ process that is mediated by an interaction Hamiltonian \mathcal{H}_I and results in the emission or absorption of some light quanta can be decomposed as

$$\begin{aligned} i\mathcal{A} &= \langle J' J'_z | \mathcal{H}_I | J J_z \rangle \\ &= \sum \langle J' J'_z | j'_\ell j'_{\ell z}; j'_h j'_{hz} \rangle \langle j'_\ell j'_{\ell z}; j'_h j'_{hz} | \mathcal{H}_I | j_\ell j_{\ell z}; j_h j_{hz} \rangle \langle j_\ell j_{\ell z}; j_h j_{hz} | J J_z \rangle \\ &= \sum \langle J' J'_z | j'_\ell j'_{\ell z}; j'_h j'_{hz} \rangle \langle j'_\ell j'_{\ell z} | \mathcal{H}_I | j_\ell j_{\ell z} \rangle \langle j_\ell j_{\ell z}; j_h j_{hz} | J J_z \rangle \delta_{j_h j'_h} \delta_{j_{hz} j'_{hz}} \end{aligned} \quad (2.1)$$

where repeated angular momentum labels are summed. If the reaction proceeds through the L -th multipole of \mathcal{H}_I , the amplitude becomes proportional to the reduced matrix element $\langle j'_\ell || L || j_\ell \rangle$ and may be conveniently rewritten in terms of a $6j$ -symbol [7,8]:

$$\begin{aligned} i\mathcal{A} &= \left[\sum \langle J' J'_z | j'_\ell j'_{\ell z}; j_h j_{hz} \rangle \langle L L_z; j'_\ell j'_{\ell z} | j_\ell j_{\ell z} \rangle \langle j_\ell j_{\ell z}; j_h j_{hz} | J J_z \rangle \right] \langle j'_\ell || L || j_\ell \rangle \\ &= (-1)^{L+j'_\ell+j_h+J} \sqrt{(2j_\ell+1)(2J'+1)} \left\{ \begin{matrix} L & j'_\ell & j_\ell \\ j_h & J & J' \end{matrix} \right\} \langle L (J_z - J'_z); J' J'_z | J J_z \rangle \langle j'_\ell || L || j_\ell \rangle. \end{aligned} \quad (2.2)$$

The consequences of spin symmetry follow from this last formula. ¹

We will apply eqn. (2.2) to heavy quarkonia transitions. In order to test its validity, we first investigate charmonia and bottomonia radiative decays. We start with the electric

¹ The only $6j$ -symbols which we will need for applications of (2.2) in this letter are

$$\left\{ \begin{matrix} L & 0 & L \\ j_h & J & j_h \end{matrix} \right\} = \frac{(-1)^{L+j_h+J}}{\sqrt{(2L+1)(2j_h+1)}} \quad \text{and} \quad \left\{ \begin{matrix} L & L & 0 \\ j_h & j_h & J' \end{matrix} \right\} = \frac{(-1)^{L+j_h+J'}}{\sqrt{(2L+1)(2j_h+1)}}.$$

dipole process $^{1,3}P_J \rightarrow ^{1,3}S_{J'} + \gamma$. In the initial state, the heavy spin angular momentum $j_h = 0$ or $j_h = 1$ can be combined with the P-wave orbital angular momentum $j_\ell = 1$ to form a h_Q or χ_{QJ} quarkonium. After the $L = 1$ radiative transition, the final state contains an S-wave η_Q or ψ_Q with $j'_\ell = 0$. Eqn. (2.2) implies that the decay rate $\Gamma(^{1,3}P_J \rightarrow ^{1,3}S_{J'} + \gamma) \propto E_\gamma^3$, averaged and summed over initial and final polarizations, is independent of J and J' in the infinite mass limit. For finite mass quarkonia, the rate indirectly depends upon these angular momentum quantum numbers through formally subleading but phenomenologically important splittings between members of the S and P-wave multiplets. Taking these splittings into account, we find the following radiative partial width ratios in the $c\bar{c}$ sector: ²

$$\begin{aligned} \Gamma(\chi_{c0} \rightarrow J/\psi + \gamma) : \Gamma(\chi_{c1} \rightarrow J/\psi + \gamma) : \Gamma(\chi_{c2} \rightarrow J/\psi + \gamma) : \Gamma(h_c \rightarrow \eta_c + \gamma) \\ = 0.095 : 0.20 : 0.27 : 0.44 \end{aligned} \quad (\text{Theory}) \quad (2.3a)$$

$$= 0.092 \pm 0.041 : 0.24 \pm 0.04 : 0.27 \pm 0.03 : \text{unmeasured}. \quad (\text{Experiment}) \quad (2.3b)$$

Analogous spin symmetry predictions in the $b\bar{b}$ sector cannot be checked against data, for absolute radiative partial widths have not yet been measured. However, we can compare theoretical and experimental values for the branching fraction ratio

$$R_J = \frac{\Gamma(\chi_{bJ}(2P) \rightarrow \Upsilon(1S) + \gamma)}{\Gamma(\chi_{bJ}(2P) \rightarrow \Upsilon(2S) + \gamma)} \propto \left[\frac{E_\gamma(2P \rightarrow 1S)}{E_\gamma(2P \rightarrow 2S)} \right]^3 \quad (2.4)$$

as a function of J :

$$R_0 : R_1 : R_2 = 3.22 : 2.55 : 2.28 \quad (\text{Theory}) \quad (2.5a)$$

$$= 5.11 \pm 4.13 : 2.47 \pm 0.60 : 2.28 \pm 0.47. \quad (\text{Experiment}) \quad (2.5b)$$

We do not include the corresponding prediction for $\Gamma(h_b(2P) \rightarrow \eta_b(2S) + \gamma)/\Gamma(h_b(2P) \rightarrow \eta_b(1S) + \gamma)$ in eqn. (2.5a) since the parabolomonium phase space factors are uncertain as the $\eta_b(1S)$, $\eta_b(2S)$ and $h_b(2P)$ masses have not been experimentally measured.

We can further test spin symmetry for heavy quarkonia by considering $^{1,3}S_J \rightarrow ^{1,3}P_{J'} + \gamma$ electric dipole decays. Inserting $j_\ell = 0$, $j'_\ell = 1$ and $L = 1$ into amplitude (2.2), we find

² We use the experimentally measured paracharmion masses $M_{\eta_c} = 2979$ MeV [9], $M_{h_c} = 3526$ MeV [10,11] and $M_{\eta'_c} = 3592$ MeV [12] to predict the $\Gamma(h_c \rightarrow \eta_c + \gamma)$ and $\Gamma(\eta'_c \rightarrow h_c + \gamma)$ entries in eqns. (2.3a) and (2.6a).

$\Gamma(^3S_1 \rightarrow ^3P_{J'} + \gamma) \propto ((2J' + 1)/9) E_\gamma^3$ and $\Gamma(^1S_0 \rightarrow ^1P_1 + \gamma) \propto E_\gamma^3$. These partial width results yield the following charmonium and bottomonium sector ratios:

$$\begin{aligned} \Gamma(\psi' \rightarrow \chi_{c0} + \gamma) : \Gamma(\psi' \rightarrow \chi_{c1} + \gamma) : \Gamma(\psi' \rightarrow \chi_{c2} + \gamma) : \Gamma(\eta'_c \rightarrow h_c + \gamma) \\ = 9.3 : 7.9 : 5.4 : 1.3 \end{aligned} \quad \text{(Theory)} \quad (2.6a)$$

$$= 9.3 \pm 0.8 : 8.7 \pm 0.8 : 7.8 \pm 0.8 : \text{unmeasured} \quad \text{(Experiment)} \quad (2.6b)$$

$$\begin{aligned} \Gamma(\Upsilon(2S) \rightarrow \chi_{b0}(1P) + \gamma) : \Gamma(\Upsilon(2S) \rightarrow \chi_{b1}(1P) + \gamma) : \Gamma(\Upsilon(2S) \rightarrow \chi_{b2}(1P) + \gamma) \\ = 4.29 : 6.70 : 6.59 \end{aligned} \quad \text{(Theory)} \quad (2.7a)$$

$$= 4.3 \pm 1.0 : 6.7 \pm 0.9 : 6.6 \pm 0.9 \quad \text{(Experiment)} \quad (2.7b)$$

$$\begin{aligned} \Gamma(\Upsilon(3S) \rightarrow \chi_{b0}(2P) + \gamma) : \Gamma(\Upsilon(2S) \rightarrow \chi_{b1}(2P) + \gamma) : \Gamma(\Upsilon(2S) \rightarrow \chi_{b2}(2P) + \gamma) \\ = 7.0 : 11.3 : 12.3 \end{aligned} \quad \text{(Theory)} \quad (2.8a)$$

$$= 5.4 \pm 0.6 : 11.3 \pm 0.6 : 11.4 \pm 0.8. \quad \text{(Experiment)} \quad (2.8b)$$

Again we do not include parabottomonium partial widths in eqns. (2.7a) and (2.8a) since their symmetry breaking phase space factors are uncertain.

Comparing the theoretical and experimental numbers in eqns. (2.3) - (2.8), we see that the predictions of spin symmetry agree quite well with the quarkonia data. The discrepancies in a given $b\bar{b}$ mode are smaller than those in its $c\bar{c}$ analogue, as one would expect. Spin symmetry also works best for the lowest lying $Q\bar{Q}$ states where the ratio of the heavy quarks' kinetic energy to their rest mass is minimal. But the general success of these radiative transition findings bolsters one's confidence that results for other processes which follow from the amplitude expression in eqn. (2.2) will also work well. We therefore use it to investigate quarkonia production in the following section.

3. Orthoquarkonia Alignment

Quarkonia physics involves a number of different scales separated by the velocity v of the heavy quarks inside $Q\bar{Q}$ bound states. These scales are set by the quarks' mass M_Q , typical momentum $M_Q v$ and kinetic energy $M_Q v^2$. Within the past few years, an effective field theory formalism called Nonrelativistic Quantum Chromodynamics (NRQCD) has been established to keep track of this quarkonia scale hierarchy [13]. The effective theory

is based upon a double power series expansion in the heavy quark velocity and strong interaction fine structure constant. Its power counting rules allow one to methodically determine the most important contributions to a particular quarkonium process [14]. We will utilize these NRQCD rules in conjunction with spin symmetry arguments to investigate quarkonia production via gluon fragmentation. As we shall see, these tools yield phenomenologically interesting predictions for orthoquarkonia alignment.

We first consider $g \rightarrow \chi_{QJ}$ fragmentation. The Feynman diagrams that mediate this process at lowest order in the the velocity expansion are illustrated in figs. 1a and 1b. The graphs contribute to χ_{QJ} production through scattering collisions like $gg \rightarrow gg^* \rightarrow gg\chi_{QJ}$. Such fragmentation reactions dominate over lower order parton fusion processes when the lab frame energy q_0 of the fragmenting gluon g^* is large, but its squared four-momentum q^2 is close to the bound state's squared mass $M_{\chi_{QJ}}^2 \simeq (2M_Q)^2$. In this case, g^* is transverse up to corrections of order q^2/q_0^2 . Consequently, the fragmenting gluon is essentially real so long as its energy q_0 is significantly greater than $M_{\chi_{QJ}}$.

The $Q\bar{Q}$ states that emerge from the shaded ovals in fig. 1 reside within the first two Fock components of the χ_{QJ} wavefunction

$$|\chi_{QJ}\rangle = O(1)|Q\bar{Q}[{}^3P_J^{(1)}]\rangle + O(v)|Q\bar{Q}[{}^3S_1^{(8)}]g\rangle + \dots \quad (3.1)$$

The angular momentum quantum numbers of the $Q\bar{Q}$ pairs are indicated in spectroscopic notation inside the square brackets, and their color configurations are labeled by singlet or octet superscripts. In fig. 1a, the incoming hard gluon with four-momentum q fragments into $Q\bar{Q}[{}^3P_J^{(1)}]$ plus an outgoing hard gluon. The rate for this process is proportional to the square of the first derivative of the P-wave bound state's wavefunction evaluated at the origin $|R'_1(0)|^2 \sim v^5$. In fig. 1b, the incoming gluon turns into $Q\bar{Q}[{}^3S_1^{(8)}]$ which appears in the next-to-leading Fock component in (3.1). The formation rate for the colored S-wave pair is proportional to the square of its wavefunction $|R_8(0)|^2 \sim v^3$. The ${}^3S_1^{(8)}$ state subsequently converts to a χ_{QJ} through a soft gluon coupling which is depicted as a “black box” in fig. 1b. This “black box” may be regarded as mediating the dominant chromoelectric dipole transition ${}^3S_1^{(8)} \rightarrow {}^3P_J^{(1)} + g$. Although the resulting P-wave state has order unity overlap with the full χ_{QJ} wavefunction, the soft gluon emission costs one power of v in the amplitude and two in the rate. The total transition in fig. 1b therefore proceeds at $O(v^5)$. Alternatively, the “black box” may be viewed as combining the ${}^3S_1^{(8)}$ $Q\bar{Q}$ pair with a soft gluon to form the complete $|Q\bar{Q}[{}^3S_1^{(8)}]g\rangle$ Fock component in eqn. (3.1)

which has $O(v)$ overlap with $|\chi_{QJ}\rangle$. This interpretation again leads one to conclude that the transition in fig. 1b takes place at $O(v^5)$ [6].

Although the Feynman diagrams in fig. 1 are the same order in the NRQCD velocity expansion, their dependence upon the short distance fine structure constant is different. The graphs in fig. 1a involve two hard gluons and are suppressed by $\alpha_s(2M_Q)/\pi$ relative to the graph in fig. 1b which has only one. This perturbative QCD suppression is partly offset by the numerical values $H_1 \simeq 15$ MeV and $H'_8 \simeq 3$ MeV for the nonperturbative matrix elements associated with the color-singlet and octet graphs [6]. However, prompt χ_{QJ} production at high transverse momenta is known to be dominated by gluon fragmentation to $Q\bar{Q}[^3S_1^{(8)}]$ [15–17]. Therefore, we will simply neglect the subleading contributions to $g \rightarrow \chi_{QJ}$ which come from the diagrams in fig. 1a.³

The intermediate $^3S_1^{(8)}$ state in fig. 1b has the same quantum numbers as the incoming hard gluon. In particular, it is transversely aligned at high energies. Spin symmetry fixes the degree to which the final χ_{QJ} inherits the color-octet state's alignment through the soft gluon processes $^3S_1^{(8)} \rightarrow ^3P_J^{(1)} + g$ or $^3S_1^{(8)} + g \rightarrow ^3P_J^{(1)}$. The populations of all the individual χ_{QJ} helicity components may be determined by setting $j_\ell = 0$, $j'_\ell = 1$ and $L = 1$ in the general amplitude expression (2.2). After a straightforward computation, we find that the helicity levels are filled according to

$$\chi_{Q0} : \chi_{Q1}^{(h=0)} : \chi_{Q1}^{(|h|=1)} : \chi_{Q2}^{(h=0)} : \chi_{Q2}^{(|h|=1)} : \chi_{Q2}^{(|h|=2)} = \frac{1}{9} : \frac{1}{6} : \frac{1}{6} : \frac{1}{18} : \frac{3}{18} : \frac{6}{18}. \quad (3.2)$$

A few points about this result should be noted. Firstly, if we compare the helicity populations in (3.2) with their unaligned counterparts

$$\chi_{Q0} : \chi_{Q1}^{(h=0)} : \chi_{Q1}^{(|h|=1)} : \chi_{Q2}^{(h=0)} : \chi_{Q2}^{(|h|=1)} : \chi_{Q2}^{(|h|=2)} = \frac{1}{9} : \frac{1}{9} : \frac{2}{9} : \frac{1}{9} : \frac{2}{9} : \frac{2}{9}, \quad (3.3)$$

we see that gluon fragmentation at high transverse momenta yields a sizable χ_{QJ} alignment. Secondly, the ratios in eqn. (3.2) are consistent with the leading color-octet terms in the polarized $g \rightarrow \chi_{cJ}$ fragmentation functions which were calculated in ref. [18]. The effect of the χ_{cJ} alignment upon the angular distribution of photons that result from the electric dipole transition $\chi_{cJ} \rightarrow J/\psi + \gamma$ as well as the induced J/ψ alignment were discussed in

³ In order to completely determine the $O((\alpha_s(2M_Q)/\pi)^2)$ contribution to $g \rightarrow \chi_{QJ}$ fragmentation, the interference between the graph in fig. 1b and its one-loop corrections must be calculated along with the diagrams in fig. 1a. Such interference terms have not been included so far in $g \rightarrow \chi_{QJ}$ fragmentation function computations.

this previous article. We will not reiterate those findings of ref. [18] here, but we note that they may be simply recovered from spin symmetry arguments. Finally, uncertainty in the numerical value for the nonperturbative matrix element H'_8 drops out from the $\chi_{QJ}^{(h)}$ ratios in (3.2). Therefore, they represent more reliable predictions than corresponding estimates for absolute $g \rightarrow \chi_{QJ}^{(h)}$ fragmentation probabilities which depend upon the presently poorly constrained H'_8 parameter.

We consider next gluon fragmentation to D-wave quarkonia. In the absence of a well-established nomenclature convention, we adopt the symbol δ_{QJ} to refer to $L = 2$ quarkonia with total angular momentum J . Quark model calculations indicate that $n = 1$ and $n = 2$ δ_{bJ} bottomonia lie below the $B\bar{B}$ threshold. On the other hand, all $n = 1$ δ_{cJ} charmonia are predicted to have masses greater than $2M_D$ but less than $M_D + M_{D^*}$ [19–21].⁴ The 1^3D_1 and 1^3D_3 states may decay to $D\bar{D}$ and are broad. But parity forbids their 1^1D_2 and 1^3D_2 counterparts from decaying to two spinless mesons. The $J = 2$ charmonia are consequently quite narrow. Gluon fragmentation to 1^1D_2 paracharmonia has been found to yield a nonnegligible $p\bar{p} \rightarrow 1^1D_2 + X$ cross section at the Tevatron [22]. Fragmentation to experimentally more accessible 1^3D_2 orthocharmonia starts at the same order in the velocity expansion but one lower order in $\alpha_s(2M_c)/\pi$. The 1^3D_2 states should therefore be produced in greater abundance.

Gluon fragmentation to δ_{QJ} orthoquarkonia proceeds at $O(v^7)$ via Feynman diagrams like those illustrated in figs. 2a, 2b and 2c. The states emerging from the shaded ovals in these graphs correspond to the $Q\bar{Q}$ pairs in the following Fock components of the δ_{QJ} wavefunction:

$$|\delta_{QJ}\rangle = O(1)|Q\bar{Q}[{}^3D_J^{(1)}]\rangle + O(v)|Q\bar{Q}[{}^3P_{J'}^{(8)}]g\rangle + O(v^2)|Q\bar{Q}[{}^3S_1^{(8)}]gg\rangle + \cdots \quad (3.4)$$

The diagrams in fig. 2a and 2b are suppressed relative to that in fig. 2c by $(\alpha_s(2M_Q)/\pi)^2$ and $\alpha_s(2M_Q)/\pi$ respectively. So the dominant contribution to $g \rightarrow \delta_{QJ}$ fragmentation comes from the Fock component that contains the S-wave color-octet state. Its subsequent conversion to δ_{QJ} through long distance processes such as ${}^3S_1^{(8)} \rightarrow {}^3D_J^{(1)} + g + g$ and ${}^3S_1^{(8)} + g + g \rightarrow {}^3D_J^{(1)}$ conserves $j_h = 1$. We can thus determine the alignment which the δ_{QJ} orthoquarkonium inherits from its transverse ${}^3S_1^{(8)}$ progenitor by setting $j_\ell = 0$, $j'_\ell = 2$

⁴ Evidence for a 3.836 GeV 1^3D_2 charmonium state has recently been reported in ref. [11].

and $L = 2$ in eqn. (2.2). We find that the individual $\delta_{QJ}^{(h)}$ helicity states are populated according to

$$\begin{aligned} & \delta_{Q1}^{(h=0)} : \delta_{Q1}^{(|h|=1)} : \delta_{Q2}^{(h=0)} : \delta_{Q2}^{(|h|=1)} : \delta_{Q2}^{(|h|=2)} : \delta_{Q3}^{(h=0)} : \delta_{Q3}^{(|h|=1)} : \delta_{Q3}^{(|h|=2)} : \delta_{Q3}^{(|h|=3)} \\ &= \frac{3}{50} : \frac{7}{50} : \frac{3}{30} : \frac{5}{30} : \frac{2}{30} : \frac{3}{75} : \frac{7}{75} : \frac{10}{75} : \frac{15}{75}. \end{aligned} \quad (3.5)$$

Once δ_{QJ} orthoquarkonia are formed, spin symmetry fixes the leading order transfer of alignment from these D-wave states to S and P-wave orthoquarkonia descendants in subsequent strong and electromagnetic decays. Consider for example the decay mode $\delta_{c2} \rightarrow J/\psi \pi\pi$ in the $c\bar{c}$ sector. This reaction conserves heavy spin angular momentum since the outgoing pions are soft. So we can again use eqn. (2.2) to compute the alignment which the final J/ψ inherits from the initial δ_{c2} :

$$\begin{aligned} J/\psi^{(h=0)} &= \text{Br}(\delta_{c2} \rightarrow J/\psi \pi\pi) \left[0 \delta_{c2}^{(h=0)} + \frac{1}{6} \delta_{c2}^{(|h|=1)} + \frac{2}{3} \delta_{c2}^{(|h|=2)} \right] \\ J/\psi^{(|h|=1)} &= \text{Br}(\delta_{c2} \rightarrow J/\psi \pi\pi) \left[1 \delta_{c2}^{(h=0)} + \frac{5}{6} \delta_{c2}^{(|h|=1)} + \frac{1}{3} \delta_{c2}^{(|h|=2)} \right]. \end{aligned} \quad (3.6)$$

The names of the helicity states in this expression denote fragmentation probabilities. Inserting the $J = 2$ D-wave results from eqn. (3.5), we deduce that $\delta_{c2} \rightarrow J/\psi \pi\pi$ feeddown produces longitudinal and transverse J/ψ 's in the ratio $J/\psi^{(h=0)} : J/\psi^{(|h|=1)} = 1 : 3.6$.

We now come to the most interesting application of spin symmetry ideas to heavy quarkonia systems. Specifically, we consider its implications for S-wave quarkonia formation. Prompt J/ψ and ψ' production at the Tevatron are currently the subject of significant theoretical and experimental interest. Previous studies have found that parton fusion alone underestimates the rate for J/ψ production at large transverse momenta by more than a factor of 10. But if fragmentation is included, the disagreement between theory and experiment reduces to roughly a factor of 2 [15–17]. The remaining discrepancy may be attributed to a number of theoretical uncertainties in perturbative QCD fragmentation function computations. The application of fragmentation ideas to J/ψ production thus represents a qualitative success.

The situation for prompt ψ' production is totally different. The prediction for $d\sigma(p\bar{p} \rightarrow \psi' + X)/dp_\perp$ at high p_\perp underestimates the measured cross section by a factor of 30 even after fragmentation is taken into account [23]. Recently, gluon fragmentation to some of the $n = 2$ χ'_{cJ} states that lie above the $D\bar{D}$ threshold has been proposed as a possible significant source of ψ' 's [18,24]. This mechanism requires an uncomfortably large radiative branching

fraction $\text{Br}(\chi'_{cJ} \rightarrow \psi' + \gamma) \simeq 5\text{-}10\%$ in order to explain the factor of 30 discrepancy between theory and data. However, a search for the photons that result from the electromagnetic transition along with an analysis of their angular distribution would at least provide a means for testing this proposal.

There is another possible resolution to the ψ' surplus problem which does not involve any charmonia states above the $D\bar{D}$ threshold [25]. Instead, the answer may lie in fragmentation to higher Fock state components within the ψ' wavefunction

$$\begin{aligned} |\psi'\rangle = & O(1)|c\bar{c}[{}^3S_1^{(1)}]\rangle + O(v)|c\bar{c}[{}^3P_J^{(8)}]g\rangle \\ & + O(v^2)|c\bar{c}[{}^3D_J^{(1,8)}]gg\rangle + O(v^2)|c\bar{c}[{}^1S_0^{(8)}]g\rangle + O(v^2)|c\bar{c}[{}^3S_1^{(1,8)}]gg\rangle + \dots \end{aligned} \quad (3.7)$$

Gluon fragmentation to the $c\bar{c}[{}^3S_1^{(1)}]$ pair in the leading Fock component starts at $O(v^3(\alpha_s(2M_c)/\pi)^3)$ via Feynman diagrams like the one illustrated in fig. 2a. Fragmentation to the $c\bar{c}$ states in all other Fock components of $|\psi'\rangle$ takes place at higher order in the velocity expansion. But the heavy charm-anticharm pairs in the subleading Fock components can be formed at lower orders in $\alpha_s(2M_c)/\pi$. In particular, the transformation shown in fig. 2c of a hard gluon into a ${}^3S_1^{(8)} c\bar{c}$ pair followed by its conversion into ψ' via the emission or absorption of two soft gluons occurs at $O(v^7\alpha_s(2M_c)/\pi)$. If we evaluate the relative strengths of the ψ' production processes in figs. 2a and 2c by setting $v^2 \simeq 0.3$ and $\alpha_s(2M_c)/\pi \simeq 9.0 \times 10^{-2}$, we find $v^3(\alpha_s(2M_c)/\pi)^3 \simeq 1.2 \times 10^{-4}$ and $v^7(\alpha_s(2M_c)/\pi) \simeq 1.4 \times 10^{-3}$. Hence, gluon fragmentation to the color-octet $c\bar{c}$ pair within the last Fock state of eqn. (3.7) may naively be an order of magnitude more important than that to the color-singlet pair within the first Fock state. If so, its inclusion could resolve the ψ' problem.⁵

Without knowing the value for the nonperturbative matrix element associated with $g \rightarrow c\bar{c}[{}^3S_1^{(8)}]$ fragmentation, we cannot draw any definite conclusion regarding this possible ψ' production mechanism. But spin symmetry provides a powerful means for testing the hypothesis that this proposal accounts for most of the prompt ψ' 's observed at the Tevatron. Recall that the ${}^3S_1^{(8)} c\bar{c}$ pair in fig. 2c is transverse up to $O(M_{\psi'}^2/q_0^2)$ corrections. This intermediate $j_\ell = 0$ state transforms at leading order in the velocity expansion into a $j'_\ell = 0$ ψ' through the $L = 0$ emission or absorption of two soft gluons. The outgoing ψ' in

⁵ Gluon fragmentation to the $c\bar{c}$ pair within the $|c\bar{c}[{}^3S_1^{(8)}]gg\rangle$ Fock component of $|\psi\rangle$ also enhances prompt J/ψ production. However, its impact is smaller than that for ψ' production since high transverse momenta J/ψ 's predominantly come from $g \rightarrow \chi_{cJ}$ fragmentation.

fig. 2c has exactly the same angular momentum quantum numbers as the incoming hard gluon. Therefore, ψ' 's produced at high transverse momenta via gluon fragmentation to the final Fock state in eqn. (3.7) are 100% transversely aligned!

This striking prediction can be tested by measuring the lepton angular distribution in the $\psi' \rightarrow \ell^+ \ell^-$ decay channel. The decay products are generally distributed according to

$$\frac{d\Gamma}{d\cos\theta}(\psi' \rightarrow \ell^+ \ell^-) \propto (1 + \alpha \cos^2 \theta) \quad (3.8)$$

where θ denotes the angle between the lepton three-momentum in the ψ' rest frame and the ψ' three-momentum in the lab frame. The parameter α ranges over the interval $-1 \leq \alpha \leq 1$ and equals unity for totally transverse ψ' 's. Subleading corrections to the infinite mass limit prediction will shift the value for α to less than one. But experimental observation of a lepton angular distribution close to $d\Gamma/d\cos\theta \propto (1 + \cos^2 \theta)$ would provide strong support for this resolution to the ψ' surplus problem.

Acknowledgments

We thank Eric Braaten and Sandip Trivedi for helpful discussions.

References

- [1] For HQET reviews, see M. Wise, “New Symmetries of the Strong Interactions”, in Proc. of the 6th Lake Louise Winter Institute, edited by B.A. Campbell, A.N. Kamall, P. Kitching and F.C. Khanna (World Scientific, Singapore, 1991); H. Georgi, “Heavy Quark Effective Theory”, in Proc. of the Theoretical Advanced Study Institute (TASI) 1991, edited by R.K. Ellis, C.T. Hill and J.D. Lykken (World Scientific, Singapore, 1992); B. Grinstein, “Lectures on Heavy Quark Effective Theory”, in High Energy Phenomenology, Proceedings of the Workshop, Mexico City 1-12 July 1991, edited by R. Heurta and M.A. Perez, (World Scientific, Singapore); M. Neubert, Phys. Rep. **245** (1994) 259.
- [2] N. Isgur and M.B. Wise, Phys. Rev. Lett. **66** (1991) 1130.
- [3] E. Braaten and T.C. Yuan, Phys. Rev. Lett. **71** (1993) 1673.
- [4] E. Braaten, K. Cheung and T.C. Yuan, Phys. Rev. **D48** (1993) 4230.
- [5] Y.-Q. Chen, Phys. Rev. **D48** (1993) 5181.
- [6] E. Braaten and T.C. Yuan, Phys. Rev. **D50** (1994) 3176.
- [7] A. Falk and M.E. Peskin, Phys. Rev. **D49** (1994) 3320.
- [8] A.R. Edmonds, *Angular Momentum in Quantum Mechanics* (Princeton University Press, Princeton, NJ 1957).
- [9] Review of Particle Properties, Phys. Rev. **D50**, Part I (1994).
- [10] T.A. Armstrong *et al.* (E760 Collaboration), Phys. Rev. Lett. **69** (1992) 2337.
- [11] L. Antoniazzi *et al.* (E705 Collaboration), Phys. Rev. **D50** (1994) 4258.
- [12] C. Edwards *et al.* (Crystal Ball Collaboration), Phys. Rev. Lett. **48** (1982) 70.
- [13] G.T. Bodwin, E. Braaten and G.P. Lepage, ANL-HEP-PR-94-24 (1994), unpublished and references therein.
- [14] G.P. Lepage *et al.*, Phys. Rev. **D46** (1992) 4052.
- [15] E. Braaten, M. A. Doncheski, S. Fleming and M. L. Mangano, Phys. Lett. **B333** (1994) 548.
- [16] M. Cacciari and M. Greco, Phys. Rev. Lett. **73** (1994) 1586.
- [17] D.P. Roy and K. Sridhar, CERN-TH.7329/94 (1994), unpublished.
- [18] P. Cho, S. Trivedi and M. Wise, CALT-68-1943 (1994), unpublished.
- [19] E. Eichten and F. Feinberg, Phys. Rev. **D23** (1981) 2724.
- [20] W. Buchmüller, Phys. Lett. **B112** (1982) 479.
- [21] S. Godfrey and N. Isgur, Phys. Rev. **D32** (1985) 189.
- [22] P. Cho and M. Wise, CALT-68-1954 (1994), unpublished.
- [23] CDF Collaboration, Fermilab-conf-94/136-E (1994), unpublished.
- [24] F.E. Close, RAL-94-093 (1994), unpublished.
- [25] E. Braaten, private communication.

Figure Captions

- Fig. 1. Feynman diagrams which mediate gluon fragmentation to P-wave χ_{QJ} ortho-quarkonia at order (a) $v^5(\alpha_s(2M_Q)/\pi)^2$ and (b) $v^5\alpha_s(2M_Q)/\pi$.
- Fig. 2. Feynman diagrams which mediate gluon fragmentation to D-wave δ_{QJ} ortho-quarkonia at order (a) $v^7(\alpha_s(2M_Q)/\pi)^3$, (b) $v^7(\alpha_s(2M_Q)/\pi)^2$ and (c) $v^7\alpha_s(2M_Q)/\pi$. These same diagrams also mediate gluon fragmentation to S-wave ψ_Q states at order (a) $v^3(\alpha_s(2M_Q)/\pi)^3$, (b) $v^7(\alpha_s(2M_Q)/\pi)^2$ and (c) $v^7\alpha_s(2M_Q)/\pi$. Crossed graphs in (a) and (b) are not displayed.

This figure "fig1-1.png" is available in "png" format from:

<http://arXiv.org/ps/hep-ph/9411303v1>

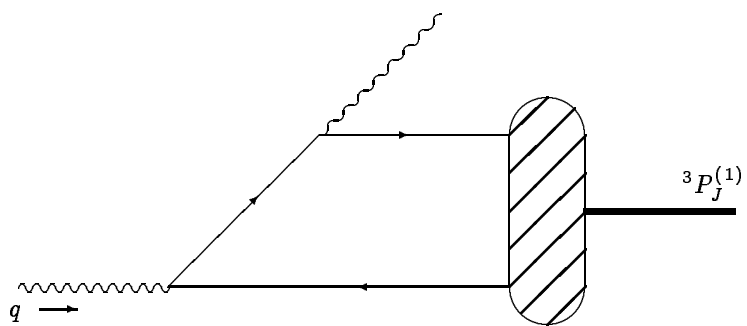
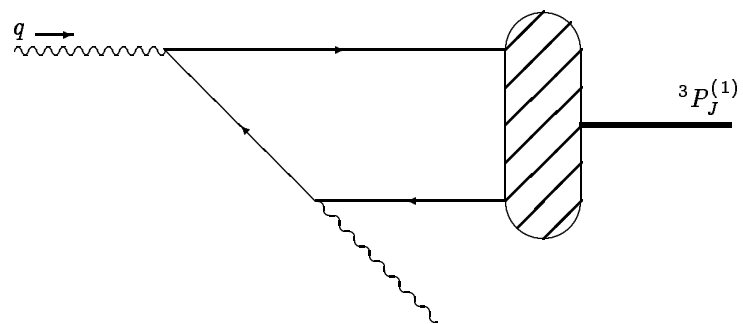


Figure 1a

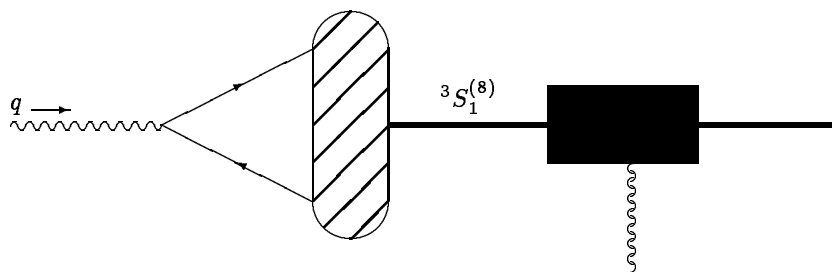


Figure 1b

This figure "fig1-2.png" is available in "png" format from:

<http://arXiv.org/ps/hep-ph/9411303v1>

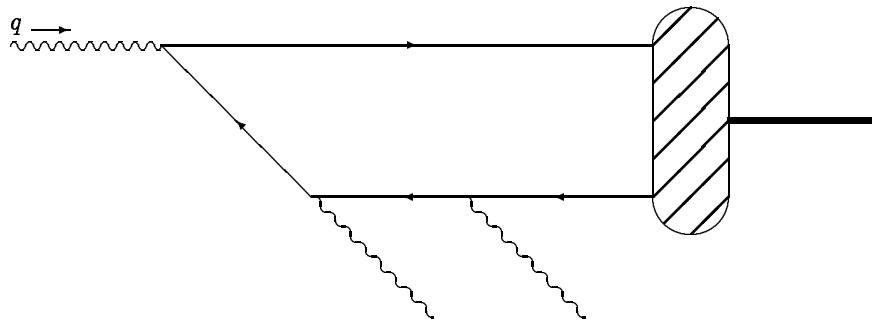


Figure 2a

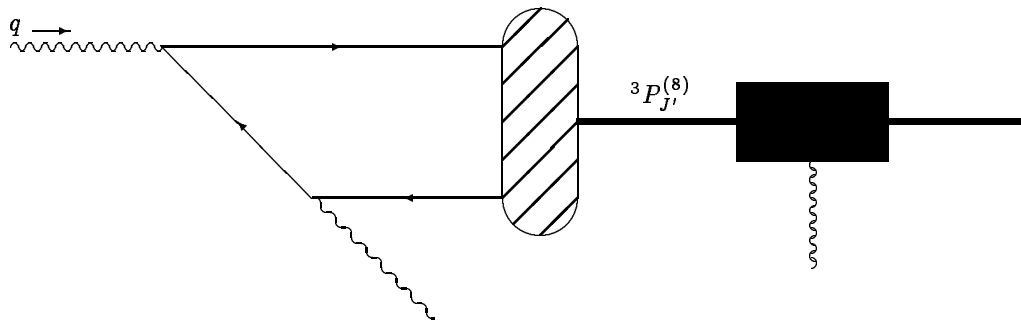


Figure 2b

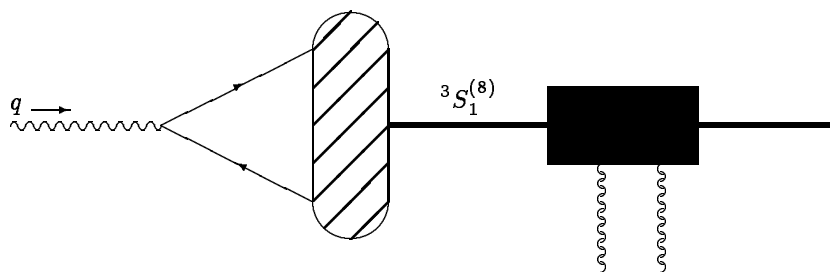


Figure 2c